Supporting Information

Engineering WTe_2@Pt Nanozyme for Machine Learning-Empowered Colorimetric H_2O_2 Detection

Meimei Xu[a], Yusi Peng[c], Yuzhen Zhao[a*], Qian Zhang[a], Rui Tian[a], Jiayin Shang[a], Teng Du[a], Cheng Ma[a], Wenqi Song[a], Zemin He[a], Zongcheng Miao[b*] and Yong Yang[c*]

[a]Xi'an Key Laboratory of Advanced photo-electronics Materials and Energy Conversion Device, Technological Institute of Materials &Energy Science (TIMES), Xijing University, Xi'an 710123, China

[b]School of Artificial Intelligence, Optics and Electronics (iOPEN), Northwestern Polytechnical University, Xi'an, 710072, PR China

[c]State Key Laboratory of High-Performance Ceramics and Superfine Microstructures, Shanghai Institute of Ceramics, Chinese Academy of Sciences, 1295 Dingxi Road, Shanghai 200050, People's Republic of China

[*]Corresponding authors: Yuzhen Zhao: zyz19870226@163.com; Zongcheng Miao: miaozongcheng@nwpu.edu.cn; Yong Yang: yangyong@mail.sic.ac.cn

1. Reagents and instruments

1.1 Reagents

Telluride tungsten (WTe_2) powder, ascorbic acid ($C_6H_8O_6$) and chloroplatinic acid hexahydrate ($H_2PtCl_6•6H_2O$) and 3,3',5,5'-Tetramethylbenzidine (TMB) were purchased from Aladdin Bio-Chem Technology Co. Ltd. Hydrogen peroxide (H_2O_2) was supplied by Sigma-Aldrich Co. HAc-NaAc buffer solution was purchased from Ida Technology Co. Ltd. All chemicals were used as received without further purification.

1.2 Instruments

The crystal structure of the prepared materials was characterized through X-ray diffraction (XRD, D8, Bruker). The microstructural features of the prepared material were analyzed by using a transmission electron microscope (TEM, Thermo Fisher-Talos F200S) equipped with an energy-dispersive X-ray spectrometer (EDS). The atomic force microscopy (AFM, NTEGRA) was carried out to study the thickness of samples. The elemental composition was studied by using X-ray photoelectron spectroscopy (XPS, Thermo Fisher-K-Alpha). The Pt content was determined by inductively coupled plasma optical emission spectroscopy (ICP-OES, Ultima Expert). The zeta potential of materials was measured using zeta potential analyzer (Litesizer TM 500). The electron paramagnetic resonance (ESR) spectra were performed on a EMX nano spectrometer. The absorbance spectra were acquired by UV-vis-NIR spectrophotometer (Lambda1050+). The photographs during the detection process were obtained by a smart phone.

2. Experimental Section

2.1 Preparation of WTe_2 nanosheets

WTe_2 nanosheets were prepared via one-step liquid exfoliation method. Specifically, 400 mg commercial WTe_2 powder was dispersed in 40 mL deionized water and then ultrasonic vibration in an ice-water bath for 6 hours. Afterward, the supernatant was collected by centrifugation at 5000 rpm for 6 min to discard the large particles and the obtained supernatant was further centrifugated by alternately washed with deionized water and ethanol for three times to obtain WTe_2 nanosheets (10000 rpm, 6 min).

2.2 Preparation of WTe_2@Pt nanosheets

50 μL H_2PtCl_6•$6H_2O$ (20 mM) was added into 2 mL WTe_2 nanosheets solution (2 mg/mL) followed by adding 200 μL ascorbic acid solution (20 mg/mL).[1] The mixture was stirred at room temperature for 1 h. The final products were collected under centrifugation and washed with deionized water for three times (12000 rpm, 5 min). Finally, the collected products were re-dispersed in 2 mL deionized water and stored at 4 °C for further use.

2.3 Evaluation of Peroxide (POD)-like activity of WTe_2@Pt nanosheets

The POD-like activity of WTe_2@Pt was characterized based on the catalytic oxidation of TMB in the presence of H_2O_2. The typical reaction process was carried out as follows: 100 μL of TMB solution (final concentration of 0.08 mM), 100 μL of H_2O_2 solution (final concentration of 2.22 mM), and 50 μL of the WTe_2@Pt (final concentration of 0.04 mg/mL) were successively added into 2 mL of HAC-NaAc buffer. The absorption spectra were recorded after incubation for 15 min. Meanwhile, the effects of pH (3.5-7) or temperature (10-40 ℃) on the POD-like activity were investigated. Under the optimized measure conditions, the steady-state kinetics experiment was performed under varied concentrations of TMB and H_2O_2. The enzymatic kinetic parameters were determined using the Michaelis-Menten equation:[2]

$$\frac{1}{V} = \frac{K_m}{V_{max}} \frac{1}{[S]} + \frac{1}{V_{max}}$$

where V_{max} denotes the maximal reaction velocity, V represents the initial velocity, K_m is the Michaelis constant and [S] indicates the concentration of substrate.

2.4 Colorimetric detection of H_2O_2

For the colorimetric assay, 50 μL of WTe_2@Pt (2 mg/mL) and 100 μL of TMB (2 mM) were mixed with 100 μL of H_2O_2 solutions at various concentrations in 2 mL of HAC-NaAc buffer. The reaction mixture was incubated for 15 min, after which the absorbance was measured at 652 nm. The limit of detection (LOD) was calculated using the 3σ/S method, where σ represents the standard deviation of the blank signal and S is the slope of the calibration curve.

Additionally, 200 images of the reaction solution at different H_2O_2 concentrations were recorded using a smartphone. Specifically, all images were captured by the same model of smartphone (iPhone 17 Pro). To maximize inter-image comparability and minimize extraneous variability, the following standardized imaging protocols were rigorously implemented: ❍All samples were photographed under the same indoor light source; ❍A fixed focal length of 28 mm was employed, with autofocus and auto-white-balance functions enabled to maintain optical consistency while accommodating minor sample variations; ●The smartphone was mounted on a stable, adjustable tripod positioned at a fixed distance of approximately 20 cm from the sample, ensuring consistent perspective, and working distance across all acquisitions; ❍All samples were placed in identical centrifuge tubes (5 mL) against a uniform background.

Then, the information of obtained images was extracted using RF algorithm to achieve the prediction of unknown sample concentrations. To ensure model generalizability and prevent data leakage, a strict separation between training and test sets was maintained throughout the modeling process. The training set with 120 samples was used exclusively for model construction and hyperparameter tuning, while the test set with 80 samples was reserved for final model evaluation. A 5-fold cross-

validation strategy was implemented to ensure robustness. The model performance was evaluated using coefficient of determination (R^2), root mean square error (RMSE), and mean absolute error (MAE).

2.5 Detection of H_2O_2 in real sample

Spike recovery experiments were performed using milk sample to evaluate the practical applicability of WTe_2@Pt-based colorimetric sensors according to the reported literature.[3] The detailed experimental process is as follows:

① Prepare 2 mL of 1 M H_2O_2 stock solution. Briefly, 204 μL of H_2O_2 was added into 1796 μL of deionized water in a centrifuge tube and mixed thoroughly.

② Prepare milk samples. The milk was purchased from a local supermarket. To prepare the milk samples, 10 mL milk was centrifuged for 30 min at 10000 r/min to remove the fat. The resulting defatted milk was diluted tenfold with deionized water.

③ Spiking of H_2O_2 into milk samples. 15.8 μL, 22.5 μL, and 45 μL of 1 M H_2O_2 solution were added into centrifuge tubes containing 1984.2 μL, 1977.5 μL, and 1955 μL of the diluted milk sample, respectively.

④ Colorimetric detection was performed using the same procedure as above. Specifically, 50 μL of WTe_2@Pt (2 mg/mL) and 100 μL of TMB (2 mM) were mixed with 100 μL of the spiked milk samples in 2 mL of HAC-NaAc buffer. The reaction mixture was incubated for 15 min before measuring the absorbance at 652 nm. The 100 μL spiked milk sample was diluted 22.5-fold in the 2250 μL total reaction system, giving final H_2O_2 concentrations of 350 μM, 500 μM, and 1000 μM.

3. Results and Discussion

The chemical states and surface composition of WTe_2@Pt were investigated by X-ray photoelectron spectroscopy (XPS). As illustrated in Fig. S2a, the peaks of W $4f_{5/2}$ and W $4f_{7/2}$ were respectively located at 33.79 eV and 31.67 eV, indexing to the W-Te bonds.[4] The peaks exhibited a negative shift of about 0.1 eV compared to the WTe_2 nanosheets. Meanwhile, the similar shift was also observed for the Te $3d_{3/2}$ (583.22 eV) and Te $3d_{5/2}$ (572.88 eV) of WTe_2@Pt nanosheets (Fig. S2b), providing direct evidence

of electron transfer from Pt to WTe_2.[5] This phenomenon can be attributed to the difference in work function between metallic Pt and WTe_2, which derived electron redistribution at the interface upon forming the heterostructure. The increased electron density on WTe_2 is expected to facilitate the adsorption and activation of H_2O_2 molecules, thereby accelerating the catalytic reaction. Additionally, there were W-O and Te-O bonds were observed due to the surface oxidation in the ambient environment. For Pt analysis in Fig. S2c, two photoelectron peaks at binding energies of 74.89 eV and 71.57 eV attributed to Pt $4f_{5/2}$ and $4f_{7/2}$ regions, and both metallic Pt^0 and Pt^{2+} existed in the WTe_2@Pt nanosheets. The result was similar with previous reported Pt related composites.[6]

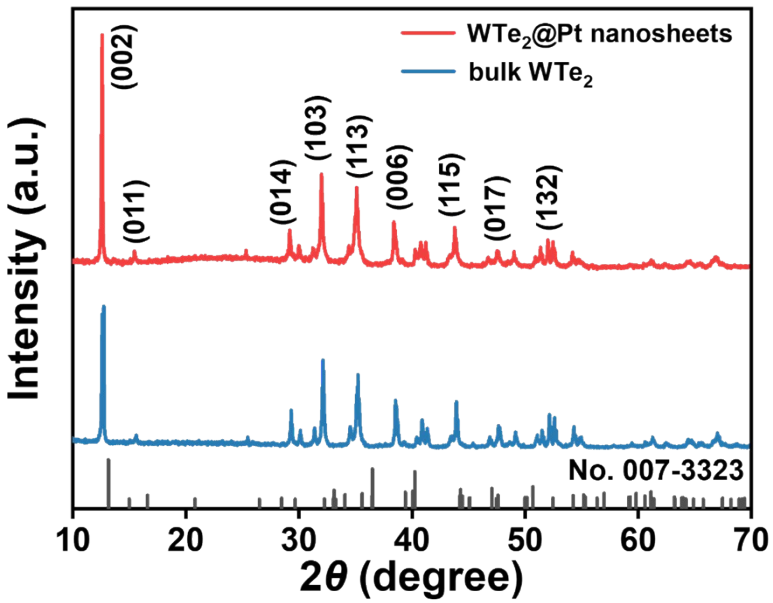

Fig. S1 XRD patterns of bulk WTe_2 and WTe_2@Pt nanosheets.

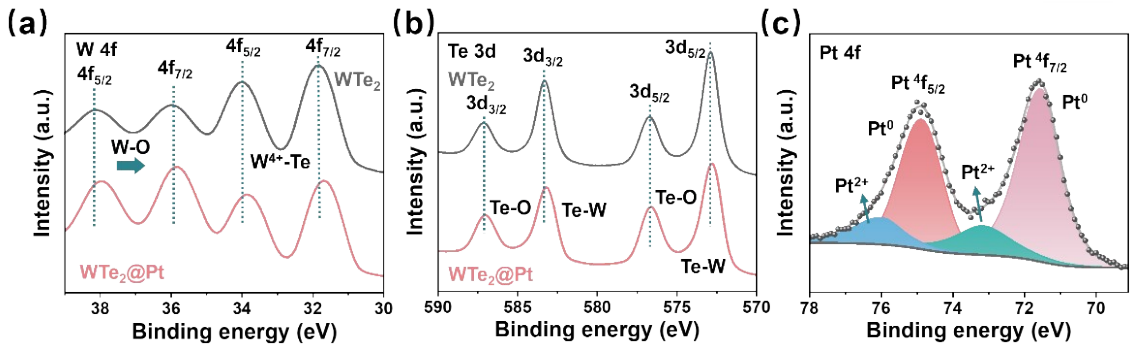

Fig. S2 The high-resolution XPS spectrum of W (a), Te (b), and Pt (c) for WTe_2 and WTe_2@Pt.

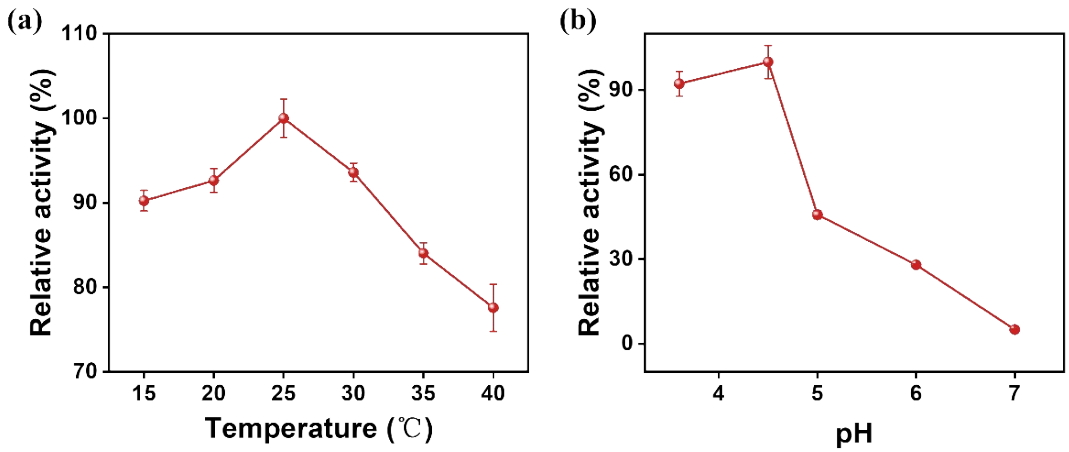

Fig. S3 Relative POD-like catalytic stabilities of WTe_2@Pt nanosheets under different temperatures and pH values.

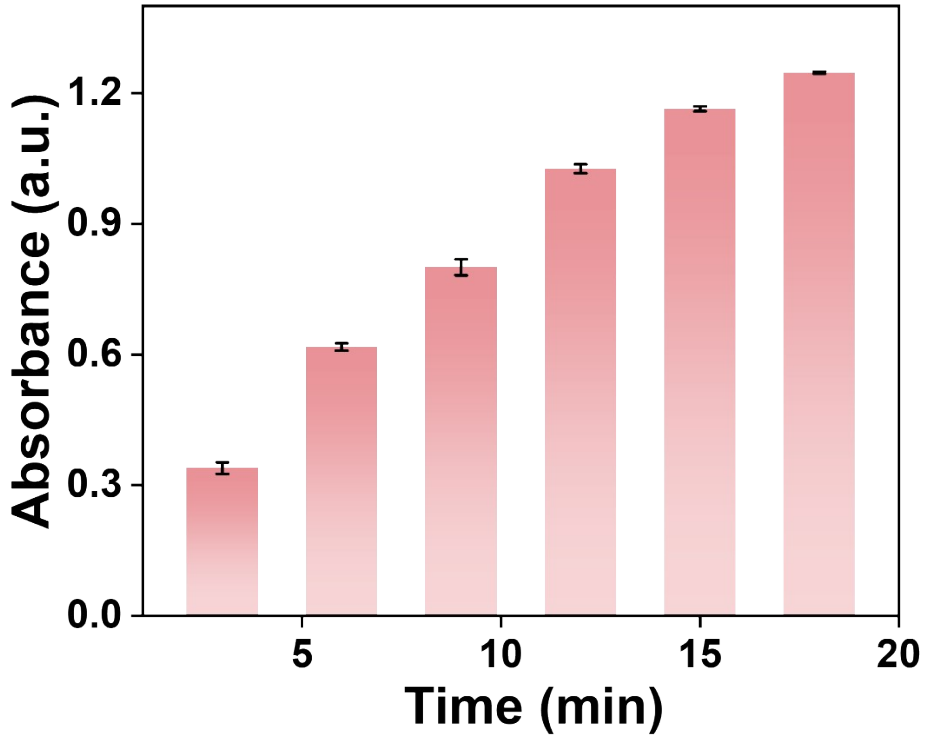

Fig. S4 Catalytic performance of WTe_2@Pt nanosheets at various time.

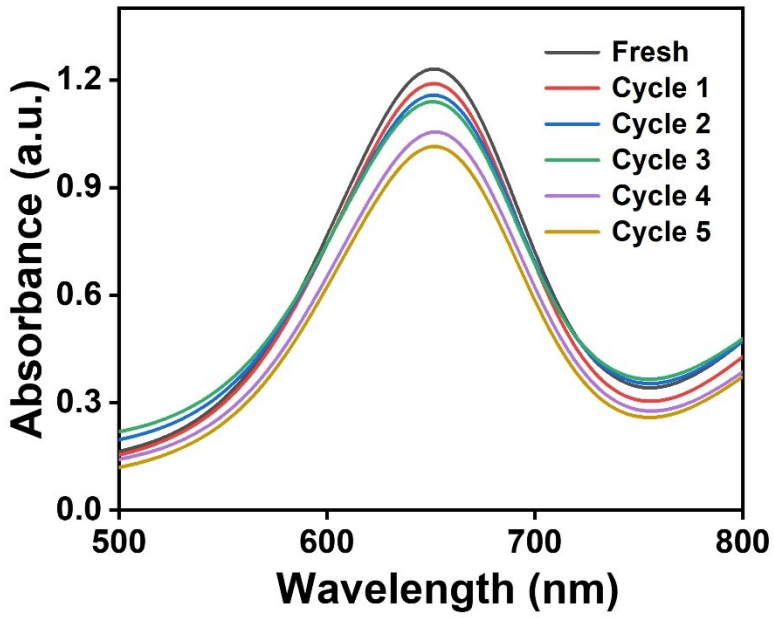

Fig. S5 Cycle stability of the POD-like activity of WTe_2@Pt after five consecutive catalytic cycles, using an assay system containing 50 μL of WTe_2@Pt in acetate buffer (pH 4.5), 2 mM TMB and 100 mM H_2O_2.

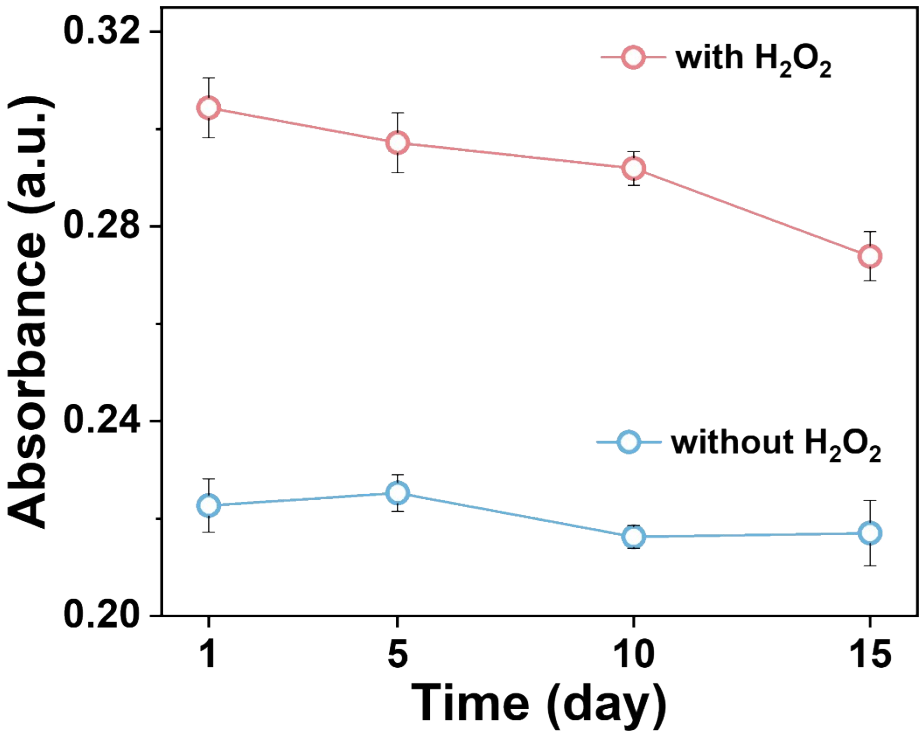

Fig. S6 Detection performance of WTe_2@Pt nanosheets after storage for 15 days.

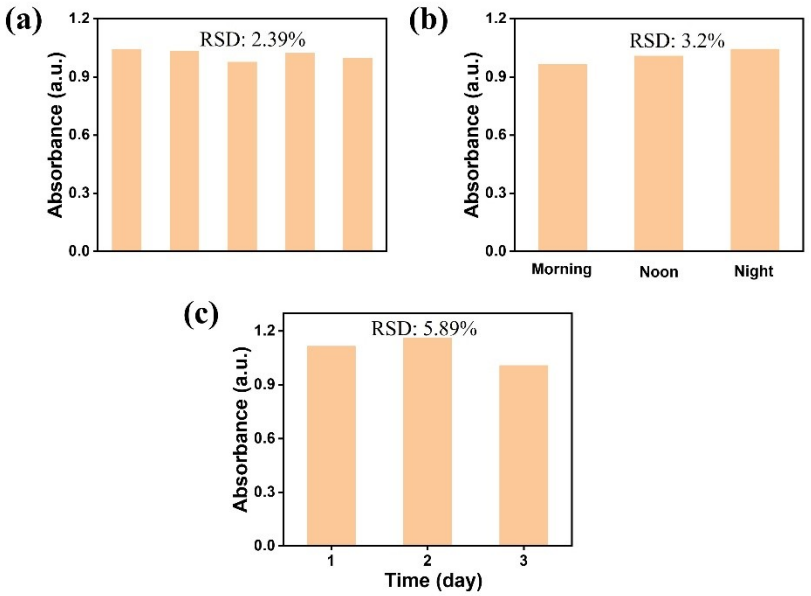

Fig. S7 (a) Results of colorimetric in five independent experiments at concentrations of 1500 μM. Stability assessment of the POD-like activity of WTe_2@Pt for H_2O_2 detection, (b) intra-day assay, (c) inter-day assay.

Table S1. Comparison of the kinetic parameters of different TMD-based nanozymes and HRP.

Nanozyme	Substrates	K_m (mM)	V_{max} (10^{-7} M s^{-1})	Ref
HRP	H_2O_2	3.7	1.0	[7]
	TMB	0.43	0.87	
WS_2/graphene oxide	H_2O_2	10.001	0.09332	[8]
	TMB	22.406	0.09606	
2D Fe-BTC	H_2O_2	0.0334	0.265	[9]
	TMB	0.2610	0.795	
Cu_2O/Au–Pt@MOF@F127	H_2O_2	22.4	0.405	[10]
Mn-CeO_2	H_2O_2	8.67	0.752	[11]
	TMB	0.25	0.845	
MoS_2/g-C_3N_4	H_2O_2	1.32	0.727	[12]
	TMB	0.15	1.302	
WTe_2@Pt	H_2O_2	0.49	0.89	This work
	TMB	1.13	2.01	

Table S2. Comparison of different colorimetric sensors for H_2O_2 assays.

Material	Linear range (μM)	LOD (μM)	Ref
FeCo-CDs	200-1500	0.77	[13]
CuO	4.6-769	0.109	[14]
Fe-aminated lignin	10000-100000	54	[15]
Co_3O_4@C	100-1000	4.08	[16]
	1000-5000		
Au/Pt/$Ti_3C_2Cl_2$	50-10000	10.24	[17]
Cu-BDC@$FeMo_6$	300-900	10	[18]
WTe_2@Pt	200-2000	9.9	This work

Table S3. The result of hyperparameter tuning.

	n_estimators	max_depth	min_samples_split	min_samples_leaf	RMSE
1	50	None	2	1	286.69
2	100	None	2	1	285.38
3	200	None	2	1	287.63
4	50	None	5	1	288.19
5	100	None	5	1	286.37
6	200	None	5	1	289.25
7	50	None	2	2	285.99
8	100	None	2	2	282.87
9	200	None	2	2	286.7
10	50	None	5	2	285.6
11	100	None	5	2	283.74
12	200	None	5	2	287.1
13	50	15	2	1	286.69
14	100	15	2	1	285.38
15	200	15	2	1	287.63
16	50	15	5	1	288.19
17	100	15	5	1	286.37
18	200	15	5	1	289.25
19	50	15	2	2	285.99
20	100	15	2	2	282.87
21	200	15	2	2	286.7
22	50	15	5	2	285.6
23	100	15	5	2	283.74
24	200	15	5	2	287.1
25	50	30	2	1	286.69
26	100	30	2	1	285.38
27	200	30	2	1	287.63
28	50	30	5	1	288.19
29	100	30	5	1	286.37
30	200	30	5	1	289.25
31	50	30	2	2	285.99
32	100	30	2	2	282.87
33	200	30	2	2	286.7
34	50	30	5	2	285.6
35	100	30	5	2	283.74
36	200	30	5	2	287.1

References

[1] X. Lai, G. Zhang, L. Zeng, X. Xiao, J. Peng, P. Guo, W. Zhang and W. Lai, ACS Appl. Mater. Interfaces, 2020, **13(1)**, 1413-1423.

[2] Y. Wang, S. Tian, S. Chen, M. Li and D. Tang, Anal. Chem., 2025, **97(13)**, 7526-7535.

[3] F. Zhang, J. Chen, F. Zhao, M. Liu, K. Peng, Y. Pu, Y. Sang, S. Wang and X. Wang, Biosens. Bioelectron., 2024, **252**, 116139.

[4] S. Li, F.C. Lei, X. Peng, R.Q. Wang, J.F. Xie, Y.P. Wu and D.S. Li, Inorg. Chem. 2020, **59 (17)** 11935-11939.

[5] C. Du, Z. Yang, A. Mo, X. Duan and G. Yang, Nano Res., 2023,**16 (8)** 10976-10984.

[6] X. Lin, P. Zhou, Q. Li and Y. Pang, Anal. Chem., 2024, **96 (26)** 10686-10695.

[7] E. Vilian, J. Ahn, A. Mohammadi, S.R. Hormozi Jangi, L. Mohammadzadeh, J. Choo, Y.S. Huh and Y.K. Han, Biosens. Bioelectron., 2026, **295**, 118287.

[8] S. Keerthana, A. Rajapriya, C. Viswanathan and N. Ponpandian, J. Alloy. Compd., 2021, **889**, 161669.

[9] A. Yuan, Y. Lu, X. Zhang, Q. Chen and Y. Huang, J. Mater. Chem. B., 2020, **8 (40)** 9295-9303.

[10] Y. Cheng, Y. D. Xia, Y. Q. Sun, Y. Wang and X. B. Yin, Adv. Mater., 2023, **36 (8)** 2308033.

[11] R. Wang, B. Guan, W. Wang, H. Yan, J. Jin, Y. Yang, L. Li, L. Guo and Y. Zeng, Sensor. Actuat. B- Chem., 2025, **427**, 137178.

[12] X. Liu, L. Huang, Y. Wang, J. Sun, T. Yue, W. Zhang and J. Wang, Sensor. Actuat. B- Chem., 2020, **306**, 127565.

[13] S. Wu, Z. Yu, J. Zhao, Y. Wang, J. Nan, L. Xu, X. Li, L. Yang and S. Dong, Anal. Chem., 2025, **97 (28)** 15320-15328.

[14] R. Singh, R. Kumari, C.S.P. Tripathi and D. Guin, Spectrochim. Acta. A., 2024,

321, 124720.

[15] L. Li, X. Liu, R. Zhu, B. Wang, J. Yang, F. Xu, S. Ramaswamy and X. Zhang, ACS Sustainable Chem. Eng., 2021, **9 (38)** 12833-12843.

[16] M. Shao, Y. Xu, Q. Shi, Y. Guo, F. Guo, H. Zeng, C. Li and M. Chen, Microchem. J., 2024, **205**, 111363.

[17] X. Xi, J. Wang, Y. Wang, H. Xiong, M. Chen, Z. Wu, X. Zhang, S. Wang and W. Wen, Carbon 2022, **197**, 476-484.

[18] Y. Xu, J. Zhou, P. Sun, P. Li, D. Han, X. Wang and F. Chai, Purif.Technol., 2025, **353** 128396.